Acta Pharmaceutica Sinica B 2021;11(7):1978−1992

Chinese Pharmaceutical Association
Institute of Materia Medica, Chinese Academy of Medical Sciences

Acta Pharmaceutica Sinica B

www.elsevier.com/locate/apsb
www.sciencedirect.com

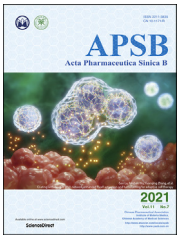

ORIGINAL ARTICLE

Gold nanorods-mediated efficient synergistic immunotherapy for detection and inhibition of postoperative tumor recurrence

Yingying Zhang[a,b], Tiange Wang[a,b], Yu Tian[a,b], Chaonan Zhang[a,b], Kun Ge[c], Jinchao Zhang[c], Jin Chang[a,b,*], Hanjie Wang[a,b,*]

[a]*School of Life Sciences, Tianjin University, Tianjin 300072, China*
[b]*Tianjin Engineering Center of Micro-Nano Biomaterials and Detection-Treatment Technology, Tianjin Key Laboratory of Function and Application of Biological Macromolecular Structures, Tianjin 300072, China*
[c]*College of Chemistry & Environmental Science, Key Laboratory of Medicinal Chemistry and Molecular Diagnosis of the Ministry of Education, Chemical Biology Key Laboratory of Hebei Province, Hebei University, Baoding 071002, China*

Received 17 November 2020; received in revised form 31 January 2021; accepted 4 February 2021

KEY WORDS

Synergistic immunotherapy;
Post-surgical tumor recurrence;

Abstract Tumor recurrence after surgery is the main cause of treatment failure. However, the initial stage of recurrence is not easy to detect, and it is difficult to cure in the late stage. In order to improve the life quality of postoperative patients, an efficient synergistic immunotherapy was developed to achieve early diagnosis and treatment of post-surgical tumor recurrence, simultaneously. In this paper, two kinds of theranostic agents based on gold nanorods (AuNRs) platform were prepared. AuNRs and

Abbreviations: AFP, alpha fetoprotein; anti-PDL1, anti-programmed cell death-ligand 1; aPDL1-LA, anti-PDL1-modified liposomes encapsulated AuNRs; aPDL1-LA+NIR, anti-PDL1-modified liposomes encapsulated AuNRs with near-infrared irradiation; aPDL1-LAI, anti-PDL1-modified liposomes loaded with ICG and encapsulated AuNRs; AP1-QDs, CEA aptamer-modified CdTe QDs; AP2-AuNRs, CEA aptamer-modified AuNRs; $CdCl_2$, cadmium chloride; CA, cancer antigen; CEA, carcinoembryonic antigen; CdTe QDs, CdTe quantum dots; CTAB, cetrimonium bromide; CTCs, circulating tumor cells; DC, dendritic cells; DLS, dynamic light scattering; EDC, 1-ethyl-3-(3′-dimethylaminopropyl) carbodiimide; FBS, fetal bovine serum; FRET, fluorescence resonance energy transfer; GSH, glutathione; AuNRs, gold nanorods; $HAuCl_4$, gold chloride; Helf, human embryonic lung fibroblasts lines; Hydrogel+IFN-γ, thermal responsive hydrogels loaded with interferon-γ; Hydrogel+IFN-γ+QA, thermal responsive hydrogels co-loaded with AP1-QDs; AP2-AuNRs, and interferon-γ; ICG, indocyanine green; IFN-γ, interferon-γ; IR, infrared; LA, liposomes encapsulated AuNRs; LA+NIR, liposomes encapsulated AuNRs with near-infrared irradiation; LAI, liposomes loaded with ICG and encapsulated AuNRs; LLC, murine lung cancer cells; MTT, 3-(4,5-dimethylthiazol-2-yl)-2,5-diphenyltetrazolium bromide; $NaBH_4$, sodium borohydride; NaHTe, sodium hydrogen telluride; NHS, *N*-hydroxysuccinimide; NIR, near-infrared irradiation; PD1, programmed cell death protein 1; PDL1, programmed cell death-ligand 1; PI, propidium iodide; PLGA-PEG-PLGA, thermal responsive hydrogel; PTT, photothermal therapy; QDs, quantum dots; $AgNO_3$, silver nitrate; TEM, transmission electron microscope.

*Corresponding authors.
E-mail addresses: jinchang@tju.edu.cn (Jin Chang), wanghj@tju.edu.cn (Hanjie Wang).

Peer review under responsibility of Chinese Pharmaceutical Association and Institute of Materia Medica, Chinese Academy of Medical Sciences.

https://doi.org/10.1016/j.apsb.2021.03.035

Theranostics;
Gold nanorods;
Photothermal therapy;
Lung metastasis;
Fluorescence resonance energy transfer;
Carcinoembryonic antigen

quantum dots (QDs) in one agent was used for the detection of carcinoembryonic antigen (CEA), using fluorescence resonance energy transfer (FRET) technology to indicate the occurrence of *in situ* recurrence, while AuNRs in the other agent was used for photothermal therapy (PTT), together with anti-PDL1 mediated immunotherapy to alleviate the process of tumor metastasis. A series of assays indicated that this synergistic immunotherapy could induce tumor cell death and the increased generation of $CD3^+$/$CD4^+$ T-lymphocytes and $CD3^+$/$CD8^+$ T-lymphocytes. Besides, more immune factors (IL-2, IL-6, and IFN-γ) produced by synergistic immunotherapy were secreted than mono-immunotherapy. This cooperative immunotherapy strategy could be utilized for diagnosis and treatment of postoperative tumor recurrence at the same time, providing a new perspective for basic and clinical research.

1. Introduction

With the development of technology, the surgical techniques have been improved. Malignant tumor resection is one of the leading treatment alternatives in the clinic, and has brought much hope for patients[1]. While recurrence or metastasis within the next 5 years can lead to a higher tumor mortality. Therefore, we should pay attention to the postoperative period, in which recurrence is probably occurred due to local residual tumor micro-infiltration and circulating tumor cells (CTCs)[2–5]. In addition, the local growth or tumor spread could be accelerated by perioperative trauma-related inflammation, thus inducing tumor recurrence[6,7]. However, it is difficult to detect the early stage of recurrence and cure the late stage of recurrence. What's worse, few products are clinically available to detect and inhibit recurrence after surgery, which is too expensive for patients to afford. Therefore, it is essential to develop an effective system for detecting and inhibiting postoperative tumor recurrence.

How to detect tumor recurrence after surgery? Tumor markers are chemical substances that reflect the presence of tumors. Their presence or quantitative changes may indicate the nature of the tumor, thereby contributing to tumor diagnosis, prognosis judgment, and treatment[8,9]. There were many reports about the detection of tumor markers, such as carcinoembryonic antigen (CEA)[10], alpha fetoprotein (AFP)[11], cancer antigen (CA) 125[12] and so on. Among many molecular markers, CEA is one of the tumor markers for many cancers, which can be used to indicate postoperative tumor recurrence[13]. An *in situ* controlled release system[14] could immobilize the detection system at the surgical site to detect the changes in the amount of CEA. Furthermore, residual tumor cells could spread throughout the body with blood circulation, causing metastatic recurrence[15]. Thus, it was also crucial to monitor the progress of metastasis.

When tumors are detected from important organs or tissues after surgery, reoperation is quite challenging and may not be effective enough due to the high recurrence rate[16]. Therefore, cancer therapy after surgery is also important, except for detection[17]. Postoperative consolidative therapy, including adjuvant molecular chemotherapy[18] and immunotherapy[19,20], is necessary for cancer patients. At present, immunotherapy[21,22] has become an increasingly appealing therapeutic strategy, which can not only solidify the curative effects, but also inhibit the occurrence of recurrence. Interferon-γ (IFN-γ) could inhibit the growth of cancer cells and induce cell death[23,24]. As we know, given the complex metastasis mechanisms after tumor surgery, a single treatment is difficult to achieve an efficient therapeutic effect. Therefore, synergistic immunotherapy is attractive for postoperative cancer therapy[25]. The combination of photothermal therapy (PTT) and immunotherapy[26,27] is an attractive cancer treatment because of its non-invasive and low side effects[28,29]. According to previous works, gold nanorods (AuNRs) were widely used in PTT due to their strong absorption in the near infrared region[30,31]. In addition, because of its good biocompatibility and easy surface modification, they were also used as suitable drug carriers in diagnosis[32] and biological imaging[33]. Anti-programmed cell death-ligand 1 (anti-PDL1), an immunological checkpoint inhibitor, has become an effective means of tumor immunotherapy, which can block the interaction between programmed cell death-ligand 1 (PDL1) on tumor cells and its receptors programmed cell death protein 1 (PD1) expressed on T-lymphocytes, thereby relieving immune suppression and improving anti-cancer effects[34].

Herein, an efficient synergistic immunotherapy was developed for detection and inhibition of postoperative tumor recurrence in our study. This system included two parts, as shown in Fig. 1: (1) thermoresponsive hydrogels co-loaded with interferon-γ, CEA aptamer-modified gold nanorods (AuNRs), and quantum dots (CdTe QDs) were synthesized to detect and inhibit postoperative recurrence *in situ* based on fluorescence resonance energy transfer (FRET) technology. (2) Anti-PDL1-modified liposomes encapsulated AuNRs were synthesized, which combined PTT with immunotherapy to restrain lung metastasis. Indocyanine green (ICG) was used to monitor postoperative lung metastatic recurrence. This system could kill most of the tumor cells, and numerous tumor debris were exposed and then presented to activate T cells by activated dendritic cells (DC). What's more, anti-PDL1 was combined with PDL1 highly expressed on the remaining tumor cells, followed by relieving PDL1 blockade. At last, immune cytokines were secreted by activating immune cells to exert the antitumor effects. This synergistic immunotherapy strategy could provide a new perspective for basic and clinical research.

2. Materials and methods

2.1. Materials

Thermal responsive hydrogel (PLGA-PEG-PLGA) was purchased from Dai zheng Biodegradable Materials Co., Ltd. (Jinan, China). Interferon-γ (IFN-γ) was obtained from PEPROTECH (USA). 1-Ethyl-3-(3′-dimethylaminopropyl) carbodiimide (EDC), *N*-hydroxysuccinimide (NHS), glutathione (GSH),

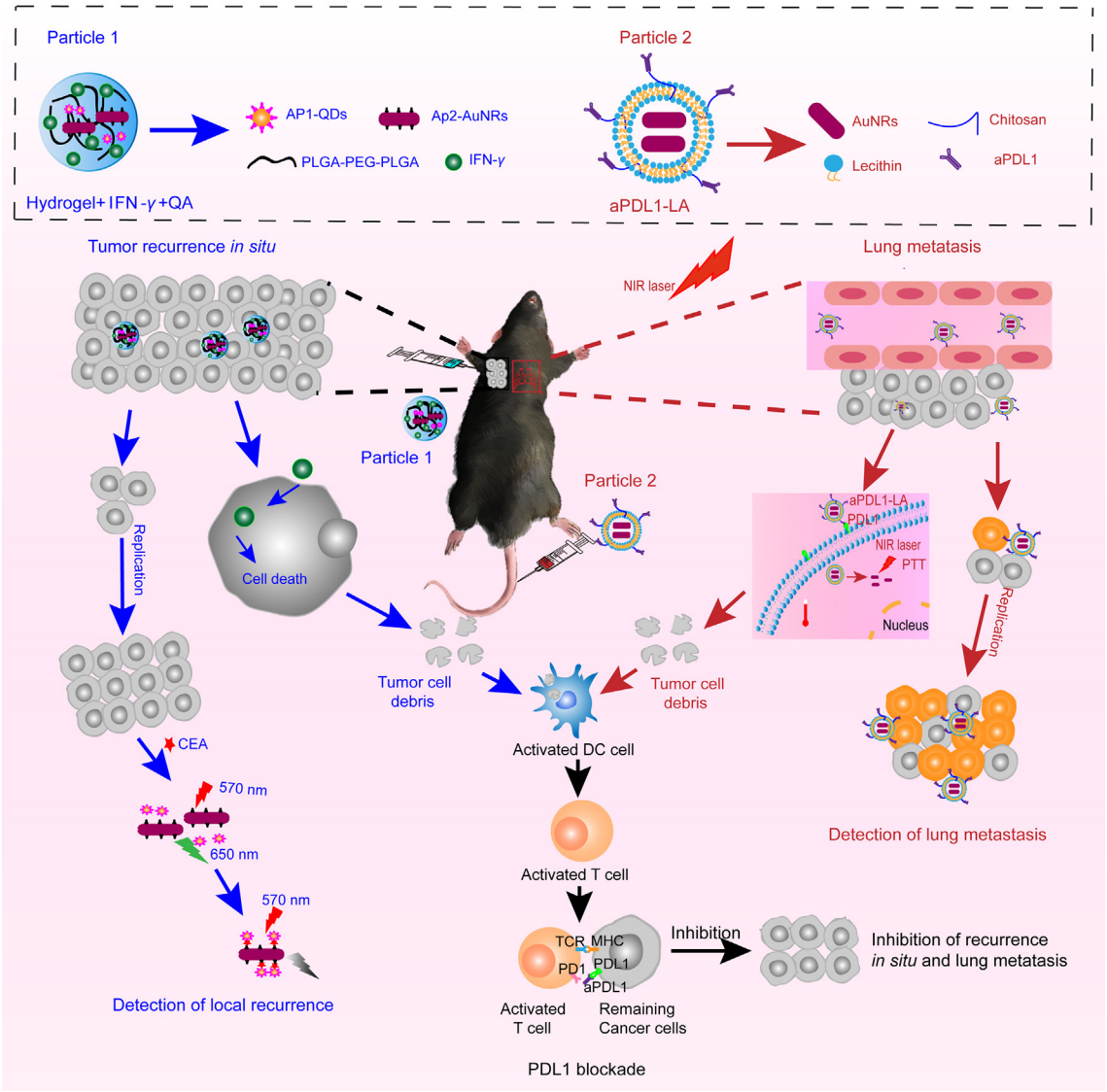

Figure 1 The scheme of the efficient synergistic immunotherapy for detection and inhibition of postoperative tumor recurrence. This system included two parts: (1) Hydrogel+IFN-γ+QA was used to detect and inhibit the postoperative recurrence *in situ* (blue). Firstly, the subcutaneous tumor was removed by operation with 5% left. Then Hydrogel+IFN-γ+QA was injected subcutaneously into the remaining tumor in the left rank. After cellular uptake, IFN-γ could inhibit tumor growth and induce tumor cells dead. Then numerous tumor debris were exposed and then presented to activated T cells by activated dendritic cells (DC). At the same time, released IFN-γ could activate the DC directly. Finally, Activated T cells would secrete immune cytokines to kill the remaining tumor cells. Besides, when the tumor cells grown, carcinoembryonic antigen (CEA) would be emitted to extracellular space. Thus CEA could combine with Ap1-CdTe QDs and AP2-AuNRs, causing the decrease of fluorescence intensity due to the fluorescence resonance energy transfer (FRET) technique. (2) The aPDL1-LA was applied to detect and inhibit the post-operative lung metastasis (red). Firstly, aPDL1-LA was intravenously injected and then arrived at lung tumor with the targeting of aPDL1. Then, aPDL1-LA could combine with the PDL1 on tumor cells surface, thus entering the tumor cells. The lung tissue was irradiated with an 808 nm laser for PTT soon afterward. Hence tumor debris was exposed and then presented to activated T cells by activated DC. What's more, aPDL1 was combined with the remaining tumor cells, followed by relieving immunosuppression. Finally, Activated T cells would secrete immune cytokines to kill tumors. To detect the lung tumor metastasis, aPDL1-LAI was injected through the tail vein. When the tumor cells grew, more aPDL1-LAI would aggregate to the tumor, leading to the increase in the fluorescence intensity of lung tissue. In a word, this efficient synergistic immuno-therapy could detect and inhibit the postoperative tumor recurrence simultaneously.

cadmium chloride ($CdCl_2$), indocyanine green (ICG), lecithin and cholesterol were bought from Aladdin Reagent Co., Ltd. (Shanghai, China). Cetrimonium bromide (CTAB), gold chloride ($HAuCl_4$), silver nitrate ($AgNO_3$) and sodium borohydride ($NaBH_4$) were achieved from Sinopharm Chemical Reagent Co., Ltd. (Shanghai, China). Propidium iodide (PI), calcein-AM, Hoechst 33258 and 3-(4,5-dimethylthiazol-2-yl)-2,5-diphenyltetrazolium bromide (MTT) were obtained from Sigma−Aldrich (Shanghai, China). Lyso Tracker Green DND-26 was brought from Invitrogen™ (USA). CEA aptamers-modified with amino and thiol were synthesized by Sango Biotech, respectively (Shanghai, China). In addition, Cy3-modified with

CEA aptamers were also synthesized from Sango Biotech (Shanghai, China). The Dulbecco's modified Eagle medium (DMEM) and trypsin were purchased from Gibco (Shanghai, China). IL-6, IL-2, IFN-γ detection kits, and Annexin V-FITC apoptosis kit were bought from Solarbio Technology Co., Ltd. (Beijing, China). Anti-mouse-CD11c-PE, anti-mouse-CD80-APC, anti-mouse-CD86-FITC, anti-mouse-CD4-FITC, anti-mouse-CD3-PE, anti-mouse-CD8-Percp were bought from Bio-Legend, Inc. (USA). In addition, CD4, CD8 and FOXP3 used for IHC analysis were bought from Abcam (UK).

2.2. Preparation of CdTe quantum dots (CdTe QDs) and gold nanorods (AuNRs)

CdTe quantum dots (CdTe QDs) were synthesized according to a published literature[35]. Cadmium chloride ($CdCl_2 \cdot 2H_2O$, 0.25 mmol) and glutathione (GSH, 0.625 mmol) were dissolved in ddH_2O (100 mL) with adjusting the pH value to 8.0 subsequently. Sodium hydrogen telluride (NaHTe, 0.0625 mmol) was added to the solution and stirred at 100 °C for 3 days. In the end, CdTe QDs were obtained by ultracentrifugation and re-dispersed in ddH_2O.

The preparation of gold nanorods (AuNRs) was performed according to previous methods[36]. After the reaction, the product was obtained by centrifugation and re-dispersed in ddH_2O.

2.3. Synthesis of CEA aptamer-modified CdTe QDs (AP1-QDs) or AuNRs (AP2-AuNRs)

CdTe QDs (2 mg) was dispersed in 4 mL MES buffer. 1.6 μmol of 1-ethyl-3-(3′-dimethylaminopropyl) carbodiimide (EDC) and 1 μmol of *N*-hydroxysuccinimide (NHS) were added at the same time. The solution was stirred for 2 h to activate the carboxyl groups of CdTe QDs, followed by centrifugation and washing with ddH_2O for three times. The carboxyl activated CdTe QDs were re-dispersed with 4 mL of HEPES buffer, and then amino-modified CEA aptamer (2 nmol, AP1) was added. The solution was stirred gently for 12 h. CEA aptamer-modified CdTe QDs (AP1-QDs) were got by centrifugation, re-dispersed in Tris−HCl buffer, and stored at 4 °C for further use.

The CEA aptamer-modified AuNRs were achieved as follows: 1 mL AuNRs solution (1 mg/mL) was reacted with 10 nmol of thiol-modified CEA aptamer (AP2) for 24 h. After the reaction, the solution was centrifuged and washed. The product (AP2-AuNRs) was re-dispersed in water.

To verify whether the CEA aptamer was successfully connected to CdTe QDs or AuNRs, Cy3-modified CEA aptamer was used. The specific experimental details were the same as above mentioned.

2.4. Synthesis of thermal responsive hydrogels co-loaded with AP1-QDs, AP2-AuNRs, and interferon-γ (IFN-γ)

PLGA-PEG-PLGA hydrogel (0.2 g) was dissolved in 1 mL ice water, and then AP1-QDs (10 mg), AP2-AuNRs (1 mg) and 10 μg of interferon-γ (IFN-γ) were added, and the solution was stirred at 4 °C. At last, the solution was put at 37 °C to form hydrogels, named as Hydrogel+IFN-γ+QA. Hydrogel+QA was obtained in the same way.

2.5. Synthesis of anti-PDL1-modified liposomes encapsulated AuNRs (aPDL1-LA)

AuNRs, which had adsorption at 808 nm, were synthesized according to a previous literature[37]. Firstly, 100 μL of anti-PDL1 (10 μmol/L) was mixed with 10 mg of EDC and 8 mg of NHS for 2 h to activate the carboxyl group, followed by centrifugation and washing. Then 200 μL of chitosan (1%, *w/v*) was reacted with activated anti-PDL1 for 12 h. After the reaction completed, the product was achieved by ultrafiltration centrifugation (MWCO = 10 kD) and named as aPDL1-Cs.

Based on previous methods[38], 5 mg of lecithin and 2.5 mg of cholesterol were dissolved in 2 mL CH_2Cl_2, and then CH_2Cl_2 was removed by rotary evaporation under vacuum. AuNRs solutions and aPDL1-Cs were added to hydrate the lipid film by ultrasound for 10 min in an ice bath. At last, the mixture was extruded through the filter membrane (0.45 μm). The obtained aPDL1-LA was stored at 4 °C for further use.

To study the cellular uptake and distribution of aPDL1-LA, ICG was introduced. The product was obtained according to the above method and named as aPDL1-LAI.

2.6. Characterization

UV−Vis absorbance was captured on a UV-2450PC Shimadzu spectroscope (Japan). Fluorescence spectra were acquired using an F280 fluorescence spectrometer (Beijing, China).

Dynamic light scattering (DLS, Malvern, UK) was used to measure the size of different nanoparticles. The infrared (IR) thermal images were captured on the Ti400 thermal imager (Fluke, USA). Transmission electron microscope (TEM) images were acquired by JEOL JEM100CXII at 180 kV (JEOL, Japan).

The successful conjugation of CEA aptamer to CdTe QDs and AuNRs was confirmed by 30% agarose gel electrophoresis. 16 μL of Cy3-modified AP1, AP1-QDs, Cy3-modified AP2, and AP2-AuNRs were mixed with 4 μL of loading buffer (5 ×), respectively. And then, all samples were subjected to 30% agarose gel electrophoresis. Images were taken using a Bio-Rad ChemiDoc MP system (BIO-RAD, USA).

Hydrogel+IFN-γ+QA, LA and aPDL1-LA dispersed in PBS were stored at 4 °C for 10 days. The changes in the particle sizes and the surface zeta potentials were monitored by DLS method.

2.7. Gel formation

According to the manufacturer's instructions, the optimum concentration range of PLGA-PEG-PLGA to form thermal responsive hydrogel is 15%−20% (*w/v*). Therefore, 0.15, 0.16, 0.17, 0.18, 0.19, and 0.2 g of PLGA-PEG-PLGA were dissolved respectively in 1 mL of ice water at 4 °C, and then the solution was put at 37 °C to form hydrogels. The gelation time was recorded.

Procedures for the CEA detection: The fluorescence spectrum of Hydrogel+QA was recorded and treated as blank group. Various concentrations of CEA standards were added, and fluorescence spectra were recorded soon afterward.

To verify the detection of cell culture medium, different quantities of murine lung cancer cells (LLC) were plated in 6-well plates. After 48 h, the cell culture medium was collected and added to Hydrogel+QA. The fluorescence spectra were measured using an F280 fluorescence spectrometer (Beijing, China).

2.8. In vitro release of IFN-γ from Hydrogel+IFN-γ+QA

Hydrogel+IFN-γ+QA were prepared at 37 °C according to above methods. Then 5 mL of ddH_2O as dissolution medium was added. 1 mL of samples was collected at certain times and equal volume of ddH_2O was supplied. The released content of IFN-γ was measured by IFN-γ detection ELISA kits.

2.9. In vitro antitumor effect of Hydrogel+IFN-γ+QA

2.9.1. MTT assay

LLC cells and human embryonic lung fibroblasts lines (Helf) were grown in DMEM supplement with 10% fetal bovine serum (FBS), 100 U/mL penicillin, and 0.1 g/mL streptomycin. Cells were cultured in a humidified 5% CO_2 atmosphere at 37 °C.

The cytotoxicity of different particles was studied using MTT assay. LLC and Helf cells were incubated with different concentrations of Hydrogel to evaluate the biocompatibility of drug carriers. Besides, LLC cells were treated with various concentrations of IFN-γ and Hydrogel+IFN-γ+QA for 24 h, and then cells were cultured with MTT solution for 4 h. At last, the absorbance was measured by a microplate reader (Thermo, MULTISCAN FC).

2.9.2. AM/PI staining

Briefly, LLC and Helf cells were grown in 48-well plates and treated with different concentrations of hydrogels for 24 h to evaluate the safety of hydrogels. Besides, LLC cells were incubated with IFN-γ and Hydrogel+IFN-γ+QA (containing 5 μg/mL of IFN-γ). After 24 h, cells were cultured with 1 μmol/L calcein-AM and PI for 15 min in the dark and then imaged by an inverted fluorescence microscope (OLYMPUS, Japan).

2.9.3. Cell apoptosis assay

In brief, LLC cells were incubated with IFN-γ and Hydrogel+IFN-γ+QA (containing 5 μg/mL of IFN-γ) for 24 h. After that, cells were stained with Annexin V-FITC and PI following the manufacturer's instructions and subjected to flow cytometry (FACSCalibur, USA).

2.10. In vivo antitumor effects of Hydrogel+IFN-γ+QA

2.10.1. In vivo imaging

Female C57BL/6 mice (about 20 g) were purchased from Beijing Charles River Co., Ltd. (China), and maintained in natural environment. All animal experiments were operated following the Guidance Suggestions for the Care and Use of Laboratory Animals and all experimental procedures were executed according to the protocols approved by Chinese Academy of Medical Science, Institute of Radiation Medicine Animal Care and Use Committee. Besides, the animal experiments were carried out following the 3 R principle (replacement, reduction and refinement).

Each C57BL/6 mouse was subcutaneously injected with 2×10^7 LLC cells. After 5 days, most of the tumors were removed surgically, with 5% left. 100 μL of Hydrogel+IFN-γ+QA (equivalence to 5 μg/mL IFN-γ) was subcutaneously injected on Day 3 after surgery. Then mice were imaged by a small animal imaging system (Maestro, USA) to evaluate the effect of inhibiting the postoperative recurrence *in situ*.

2.10.2. In vivo efficacy study

Fifteen female C57BL/6 mice were randomly divided into three groups. Each mouse was subcutaneously injected 2×10^7 LLC cells into the axilla. Then 5% of tumor tissues were left by operation after 5 days. PBS (100 μL), IFN-γ, and Hydrogel+IFN-γ+QA (equivalence to 5 μg/mL IFN-γ) were subcutaneously injected on the third day after surgery. And then the blood of mice was collected on Days 3, 5 and 8 after the operation to analyze the content of IL-6, IL-2 and IFN-γ with ELISA kits (Solarbio biotech). Besides, body weight and tumor volume were measured every other day.

2.11. Photothermal effect of aPDL1-LA

In order to explore the optimal power intensity of 808 nm laser, 20 μg/mL of AuNRs were exposed to 1.0, 1.5, 2.0 and 2.5 W/cm^2 of NIR laser for 10 min. Then temperature changes were recorded by the Ti400 thermal imager.

AuNRs and LA solutions (containing 20 μg/mL of AuNRs) were exposed to 808 nm irradiation (2.0 W/cm^2, 10 min). PBS solution was used as control. The images were captured by the Ti400 thermal imager (Fluke, USA).

2.12. Cellular uptake and lysosome escape of aPDL1-LA

aPDL1-LAI was synthesized to study the cellular uptake and lysosome escape of aPDL1-LA. Cells were incubated with LAI and aPDL1-LAI (containing 10 μg/mL of ICG) for 2 and 6 h, followed by washing with PBS to remove excess nanoparticles. Then cells were stained with 10 nmol/L of Lyso Tracker Green DND-26 at 37 °C for 1 h, cultured with 1 μg/mL of Hoechst 33258 for 15 min. In the end, the samples were observed under a laser confocal microscope (Nikon A1-ISTAR, Japan).

2.13. In vitro antitumor effects of a PDL1-LA

Helf cells were incubated with different concentrations of LA to evaluate the biocompatibility of LA by MTT assay and AM/PI staining. The cytotoxicities of aPDL1-LA with or without NIR irradiation to LLC cells were tested by MTT assay. Briefly, cells were incubated with different concentrations of AuNRs, LA and aPDL1-LA for 24 h. Then half of the cells were exposed to 808 nm laser (2.0 W/cm^2) for 5 min. Each concentration was repeated five times. The absorbance at 570 nm was measured using a microplate reader (Thermo, MULTISCAN FC). In addition, the safety of NIR laser was also considered.

2.14. In vivo antitumor effect of a PDL1-LA

2.14.1. In vivo imaging

Each female C57BL/6 mouse was intravenously injected with 2×10^6 cells to establish a lung metastasis model[39]. To verify the successful establishment of the lung metastasis model, mice were sacrificed after 15 days, and lung tissues were collected to make frozen tissue sections, followed by staining with Hoechst 33258 and imaging with an inverted fluorescence microscope (OLYMPUS, Japan). Mice injected with PBS were set as the control group. To assess the therapeutic effect, 100 μL of aPDL1-LA (containing 20 μg/mL of AuNRs) was intravenously injected on Days 1, 3 and 5. Then lung tissues were irradiated with 2.0 W/cm^2 of 808 nm laser for 5 min. Mice injected with aPDL1-LAI were imaged with a small animal imaging system (Maestro, USA) at a certain time.

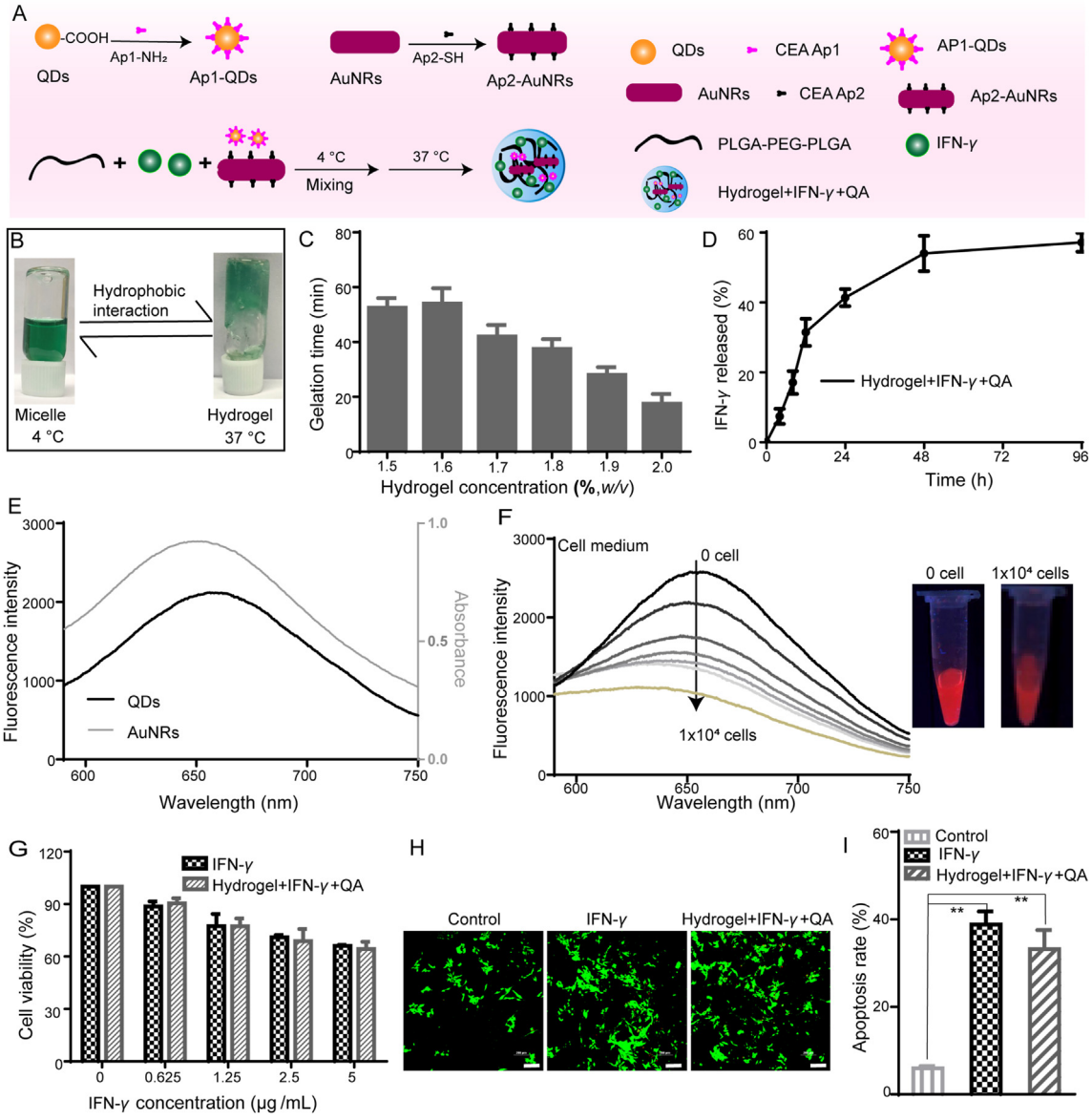

Figure 2 Characterization of Hydrogel+IFN-γ+QA and *in vitro* antitumor effects. (A) Synthesis of Hydrogel+IFN-γ+QA; (b) The phase transition images of thermal responsive hydrogel at 4 and 37 °C; (C) The gelation time changes with different concentrations of hydrogels ($n = 3$); (D) The release profiles of IFN-γ from Hydrogel+IFN-γ+QA; (E) The Fluorescence spectra of CdTe QDs at λex = 570 nm and the UV−Vis spectra of AuNRs; (F) The Fluorescence spectra and representative images of Hydrogel+IFN-γ+QA incubated with cell culture medium with different amounts of LLC cells; (G) Cell viability of LLC cells treated with IFN-γ and Hydrogel+IFN-γ+QA for 24 h ($n = 5$); (H) Calcein-AM and PI staining of LLC cells with different treatments (Scale bar = 200 μm); (I) Apoptosis analysis of LLC cells treated with IFN-γ and Hydrogel+IFN-γ+QA for 24 h ($n = 3$). Data are presented as mean ± SD; $^*P < 0.05$, $^{**}P < 0.01$ compared with control group by ANOVA analysis.

2.14.2. *In vivo efficacy study*

C57BL/6 mice were randomly divided into five groups. The establishment of lung metastasis was based on the above method. LA (100 μL) and aPDL1-LA (containing 20 μg/mL of AuNRs) were injected *via* the tail vein on Days 1, 3 and 5. The lung regions of mice were irradiated with or without 2.0 W/cm^2 of 808 nm laser for 5 min at 2 h post-injection. And then the blood was collected on Day 9 to analyze the content of IL-6, IL-2, and IFN-γ with ELISA kits. On Day 16, mice were sacrificed, and then lung tissues and lymph nodes were collected. Lung tissues were stained with hematoxylin-eosin for histological examination. Lymph nodes were collected to quantitatively analyze the levels of $CD3^+/CD8^+$ T-lymphocytes and $CD3^+/CD4^+$ T-lymphocytes by flow cytometry (FACSCalibur, USA). At the same time, mice weight was measured every two days.

2.15. *In vivo synergistic therapy*

Each C57BL/6 mouse (20 g) was intravenously injected with 2×10^6 LLC cells to establish a lung metastasis model. Then every mouse was subcutaneously injected with 2×10^7 cells 3 days later. After 5 days, most of the subcutaneous tumors were removed by surgery. 100 μL of Hydrogel+IFN-γ+QA was subcutaneously injected on Day 0. And then, 100 μL of aPDL1-LA was

intravenously injected and irradiated with 808 nm laser on Days 1, 3 and 5. Then blood was collected to analyze the content of the immune factors (IL-6, IL-2 and IFN-γ) on Day 9. At last, the main organs were collected for pathological analysis. And then lymph nodes were used to quantitatively measure the level of activated DC, $CD3^+/CD8^+$ T-lymphocytes and $CD3^+/CD4^+$ T-lymphocytes by flow cytometry (FACSCalibur, USA). At the same time, mice weight and tumor volume were measured every two days.

2.16. *Histopathology analysis and immunohistochemistry*

Main organs of mice were collected, stained with hematoxylin and eosin (H&E) and imaged by an inverted microscope (OLYMPUS, Japan).

In situ recurrence tumor sections from mice with different treatments were respectively immunostained with anti-mouse CD4, CD8 and Foxp3 proteins to analyze the content of $CD4^+$ T-lymphocytes, $CD8^+$ T-lymphocytes and Treg cells. The sections were observed by an inverted microscope (OLYMPUS, Japan).

2.17. *Statistical analysis*

All data were expressed as the mean ± SD ($n \geq 3$). Statistical analysis was performed using ANOVA analysis. When P value < 0.05, the differences were significant, $P < 0.01$, the differences were very significant.

3. Results and discussion

3.1. *Characterization and in vitro therapy of Hydrogel+IFN-γ+QA*

In order to detect and inhibit the postoperative tumor recurrence *in situ*, Hydrogel+IFN-γ+QA were synthesized as illustrated in Fig. 2A, which could be used to detect and inhibit the postoperative tumor recurrence *in situ* at the same time. In order to study the properties of the thermal responsive hydrogel, PLGA-PEG-PLGA was dissolved in ddH_2O and stored at 4 °C to accelerate the process of dissolution. ICG was introduced for the visual observation of phase transition. The thermal responsive hydrogels were in a liquid state at 4 °C, while in a gel state at 37 °C (Fig. 2B). It meant that the thermal responsive hydrogel could be subcutaneously injectable and then fixed to the tumor site. Therefore, the gelation time was important. As illustrated in Fig. 2C, the gelation time was decreased (from 55 to 18 min) with the increase of PLGA-PEG-PLGA (from 1.5% to 2.0%). 2.0% of PLGA-PEG-PLGA was used to form hydrogels in the following experiments.

The long-term stability of Hydrogel+IFN-γ+QA was characterized by monitoring the changes of surface zeta potential at 4 °C storage for 10 days. No significant changes in zeta potential were found as shown in Supporting Information Fig. S2. In this system, the *in situ* controlled release system could achieve slow drug release, which could obtain long-term antitumor effects. The drug release behaviors of IFN-γ from Hydrogel+IFN-γ+QA were studied (Fig. 2D). The release speed of IFN-γ was slightly slower. The cumulative release amount at 96 h was almost 59%. These results indicate that Hydrogel+IFN-γ+QA can achieve long-term and sustained drug release.

It is challenging to find tumor postoperative recurrence in the early stage in the clinic. Hence the detection of tumor postoperative recurrence is vital to patients. FRET is a powerful technique for the application of biological assays[40]. There were some reports about FRET technology combing CdTe QDs with AuNRs[41,42]. CdTe QDs in the NIR region were obtained for better *in vivo* imaging. The UV−Vis spectra demonstrated that AuNRs had a characteristic absorption peak at 650 nm. CdTe QDs had an emission peak at about 650 nm when excited at 570 nm. The emission of the CdTe QDs overlapped well with the absorption of AuNRs, indicating that CdTe QDs (the donor) and AuNRs (acceptor) made up an efficient FRET system (Fig. 2E). Furthermore, polyacrylamide gel electrophoresis testified the successful conjugation of CEA aptamer to CdTe QDs and AuNRs (Supporting Information Fig. S1A). The emission of Ap1-QDs and the absorption of Ap2-AuNRs were also consistent with CdTe QDs and AuNRs (Supporting Information Fig. S1B and S1C). Based on the above results, Hydrogel co-loaded with Ap1-QDs and Ap2-AuNRs was established for the detection of CEA. The fluorescence intensity of the CdTe QDs was decreased gradually with the increase of CEA (Supporting Information Fig. S1D). With the proliferation of tumor cells, an increasing number of CEA was secreted to extracellular space. Thus, cell medium with a different number of cancer cells was added, and the quenching of the CdTe QDs fluorescence occurred (Fig. 2F). *In vitro* results indicated that FRET between the CdTe QDs in the NIR region and AuNRs was successfully applied in sensing CEA.

The treatment of postoperative recurrence is favorable to the prolongation of the patient's life. MTT assay was used to evaluate the *in vitro* inhibitory effects on cell proliferation of Hydrogel+IFN-γ+QA. First of all, the safety of carriers is important in drug delivery. The unloaded hydrogels showed promising biocompatibilities in LLC cells and Helf cells (Supporting Information Figs. S3 and S4). The cell viabilities and IC50 values in presence of Hydrogel+IFN-γ+QA were similar to IFN-γ with the same concentration (Fig. 2G and Supporting Information Table S1). The AM/PI staining was also used to investigate the antitumor effect. As shown in Fig. 2H, IFN-γ showed similar red fluorescence to Hydrogel+IFN-γ+QA (containing 5 μg/mL of IFN-γ), suggesting that the loading of IFN-γ to hydrogels could not affect the antitumor effects. The apoptosis results were in correspondence with the MTT and AM/PI assays (Fig. 2I). LLC Cells incubated with free IFN-γ and Hydrogel+IFN-γ+QA displayed notable apoptosis (the apoptosis rates were about 38.8% and 33.2%, respectively).

The *in vitro* results demonstrated that Hydrogel+IFN-γ+QA could be applied not only the detection of CEA, but also the inhibition of LLC cells, which lay the foundation for *in vivo* applications.

3.2. *In vivo inhibition on postoperative recurrence of Hydrogel+IFN-γ+QA*

As we know, IFN-γ could not only directly kill the tumor. Furthermore, it could also induce strong tumor-specific immune responses. The *in vivo* antitumor effects of Hydrogel+IFN-γ+QA were investigated in the subcutaneous LLC-bearing C57BL/6 mice model. The schematic diagram of the animal experiment plan was shown in Fig. 3A. As illustrated in Fig. 3B, the fluorescence intensity of CdTe QDs was quenched by AuNRs with the proliferation of the remaining tumor cells after the operation. Tumor-bearing mice were imaged to evaluate the postoperative recurrence *in situ*. With the increase of tumor volume, the fluorescence intensity was decreased, which was in correspondence with *in vitro* results (Fig. 3C). The changes in body weight

(Fig. 3D) were insignificant, indicating the safety of all agents. The tumor volume in PBS group sharply increased and finally reached 2100 mm^3. The mice treated with IFN-γ and Hydrogel+IFN-γ+QA demonstrated significant tumor inhibitory effects (Fig. 3E and F, and Supporting Information Fig. S5). The mice in PBS group all died on Day 15. While IFN-γ and Hydrogel+IFN-γ+QA could slightly extend the survival time of mice after the operation (Fig. 3G). As shown in Supporting Information Table S2, the median survival of Hydrogel+IFN-γ group was 16 days, demonstrating that Hydrogel+IFN-γ could prolong the survival time of mice in comparison with control group.

Cytokines are a class of small molecule proteins with a wide range of biological activities secreted by immune cells. The immune response is modulated by binding to the respective receptors to regulate cell growth and differentiation[43]. Interleukin-2 (IL-2) is a cytokine with numerous biological activities and significant in regulating immune response[44]. And then IL-2 is produced exclusively by activated T cells[45]. Interleukin-6 (IL-6) can stimulate the proliferation, differentiation and function of cells involved in immune response[46]. IFN-γ has immunomodulatory and antineoplastic properties[47]. Sera were collected from LLC tumor-bearing mice after 24, 72 and 144 h treatments to measure the content of IL-2, IL-6 and IFN-γ. The amount of IL-2, IL-6 and IFN-γ induced by IFN-γ was significantly higher than Hydrogel+IFN-γ+QA at 24 h. While more IL-2, IL-6 and IFN-γ were secreted in Hydrogel+IFN-γ+QA group at 72 h, demonstrating that IFN-γ was slowly released from the hydrogel (Fig. 3H). The results indicate that Hydrogel+IFN-γ+QA can induce more secretion of immune cytokines, leading to enhanced treatment.

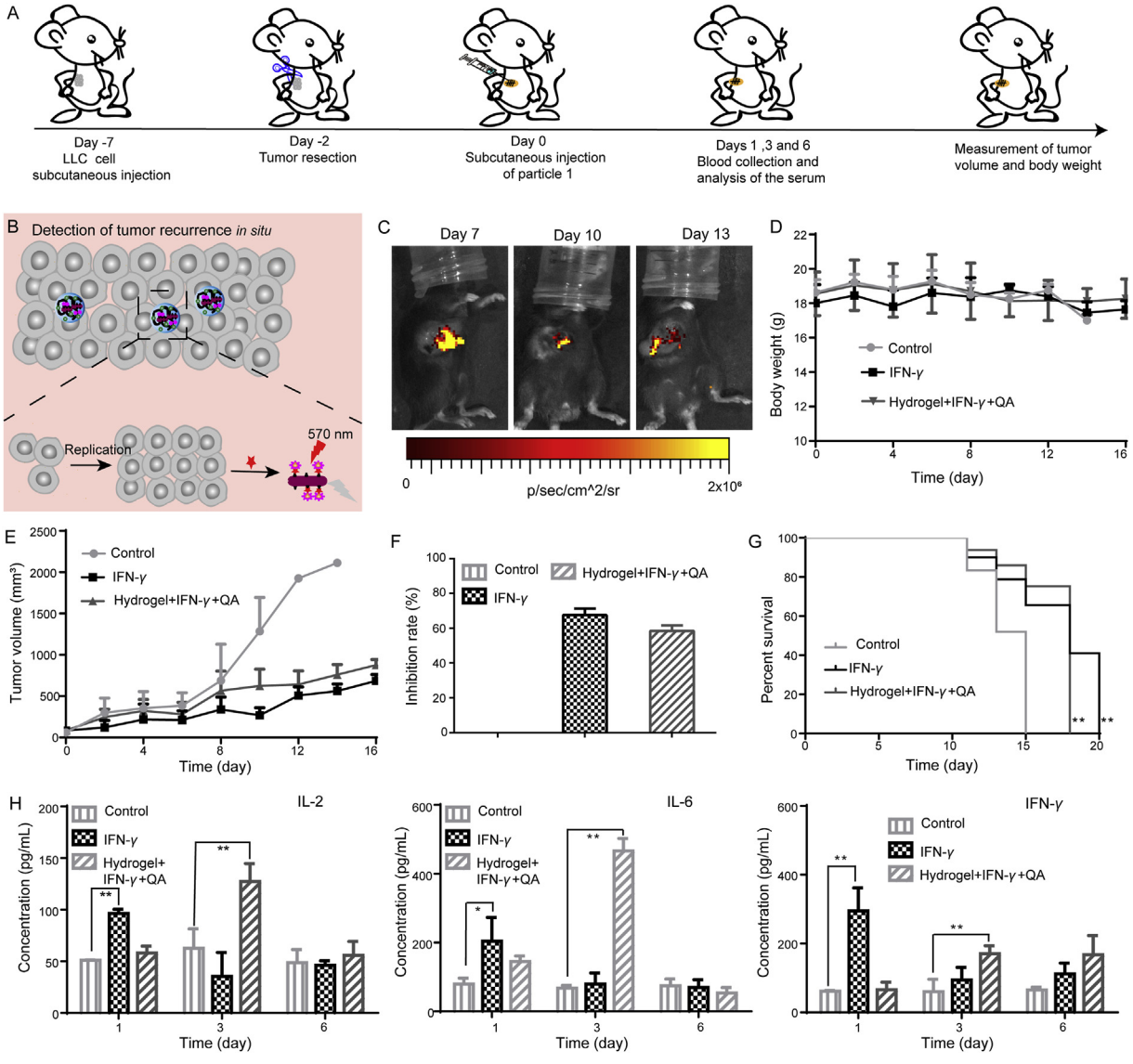

Figure 3 *In vivo* detection and inhibition of postoperative tumor recurrence *in situ*. (A) Schematic illustration of animal experiments; (B) The Schematic diagram of detection of postoperative tumor recurrence; (C) Fluorescence imaging of a subcutaneous xenograft LLC tumor model on Days 7, 10 and 13 post-injection of Hydrogel+IFN-γ+QA; (D) Body weight changes of LLC tumor-bearing mice ($n = 5$); (E) Tumor growth curves of mice with different treatments ($n = 5$); (F) Tumor inhibition rates of mice ($n = 5$); (G) Survival curves (%) of mice ($n = 5$); (H) Immune cytokine levels in sera isolated from mice on Days 1, 3 and 5 post-injection of PBS, IFN-γ and Hydrogel+IFN-γ+QA ($n = 3$). Data are presented as mean ± SD; $^*P < 0.05$, $^{**}P < 0.01$ compared with control group by ANOVA analysis.

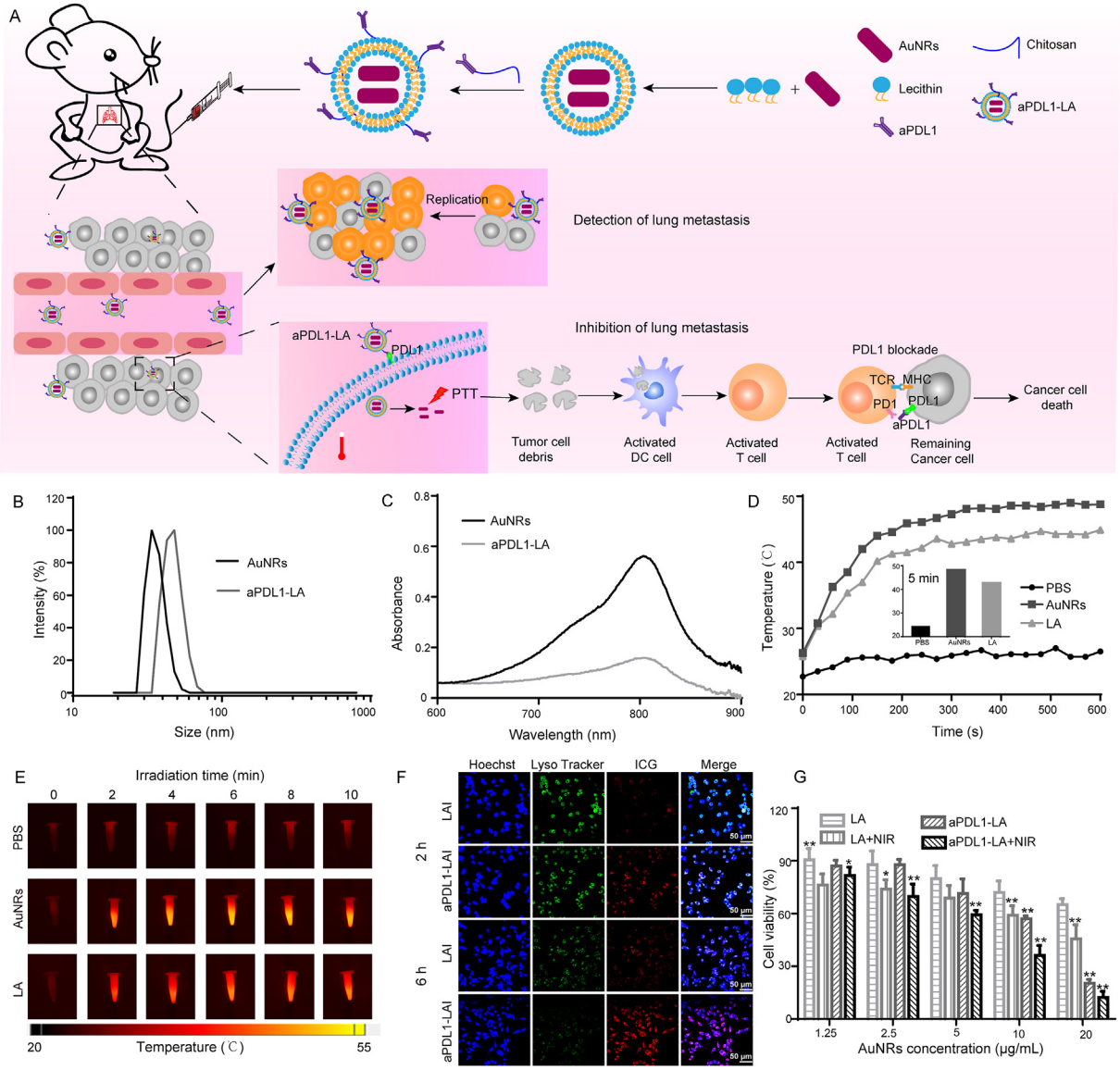

Figure 4 Synthesis and characterization of aPDL1-LA and *in vitro* inhibitory effects. (A) Schematic illustration of synthesis of aPDL1-LA and *in vivo* inhibitory effects; (B) Size distribution of AuNRs and aPDL1-LA; (C) UV−Vis spectra of AuNRs and aPDL1-LA; (D) The temperature changes of PBS, AuNRs and LA irradiated with laser at power density of 2.0 W/cm^2 for 10 min. Inset: the temperature of PBS, AuNRs and LA after 5 min of irradiation; (E) IR thermal images of PBS, AuNRs and LA; (F) Fluorescence images of LLC cells treated with LAI and aPDL1-LAI for 2 h and 6 h to evaluate the cellular uptake and lysosome escape of aPDL1-LAI (Scale bar = 50 μm); (G) Cell viability of LLC cells with different treatments for 24 h. Data are presented as mean ± SD (n = 5); *P < 0.05, **P < 0.01 compared with LA group by ANOVA analysis.

3.3. *Characterization and in vitro assay of aPDL1-LA*

The surviving tumor cells could enter the blood and then accumulate in lung tissue with blood circulation. To inhibit the lung metastasis after the operation, aPDL1-LA was synthesized, which was used for synergistic PTT and immunotherapy (Fig. 4A). As illustrated, aPDL1-LA could combine with PDL1 expressed on the cancer cell membrane and then entered the cells. Subsequently, the cells were irradiated with NIR laser for PTT. After that, the cell debris as tumor antigens could activate DC and T cells. What's more, aPDL1-LA, in combination with PDL1 expressed on remaining cancer cells, could relieve PDL1 blockade to activated T cells. Finally, lung metastasis could be inhibited by PTT and immunotherapy. DLS results demonstrated that aPDL1-LA had an average diameter of about 90 nm (Fig. 4B and Table 1). TEM images showed that AuNRs were uniform, while aPDL1-LA was unevenly dispersed and aggregated (Supporting Information Fig. S6). UV−Vis spectra suggested that AuNRs and aPDL1-LA had characteristic adsorption peak at 780 nm, indicating that AuNRs were encapsulated by liposomes (Fig. 4C).

To evaluate the optimal power intensity for PTT, AuNRs were irradiated with 808 nm laser (1.0, 1.5, 2.0 and 2.5 W/cm^2 for 10 min). As shown in Supporting Information Fig. S7, when AuNRs were irradiated with 2.0 and 2.5 W/cm^2 of 808 nm laser for 10 min, the temperatures were increased by 26.3 and 26.9 °C, respectively, while there were no obvious temperature changes when the power intensities were 1.0 and 1.5 W/cm^2. So 2.0 W/cm^2 was chosen for PTT.

In the following experiments, the temperature changes of AuNRs and LA was recorded (Fig. 4D and E). When AuNRs and

LA were incubated with 808 nm laser (2.0 W/cm^2, 10 min), the temperature had increased by 24.3 and 19.1 °C, respectively. It meant that LA could also be used for PTT. What's more, the temperature of AuNRs irradiated for 5 min was close to that of 10 min. Hence, the optimal condition for PTT was to choose the power intensity of 2.0 W/cm^2 and irradiation for 5 min. In addition, no significant changes in zeta potential and particle size of LA and aPDL1-LA were found after 10 days' storage at 4 °C, demonstrating the potential stability for cancer therapy (Supporting Information Fig. S8).

The biosafety of drug carriers is essential in drug delivery. LA showed good biocompatibilities in normal cells (Supporting Information Fig. S9). As we know, PDL1 was highly expressed in several tumor cells. To investigate the results of PDL1-mediated endocytosis, ICG was introduced to study the cellular uptake of LA and aPDL1-LA in LLC cells. As shown in Fig. 4F, the red fluorescence intensity of LLC cells increased with the prolongation of incubation time, indicating that both nanoparticles could enter the cells. Besides, the red fluorescence intensity of aPDL1-LAI was stronger than LAI, suggesting that the internalization of aPDL1-LAI into LLC cells could be PDL1-mediated. And aPDL1-LAI and LAI were distributed in the lysosomes after endocytosis. The green fluorescence of Lyso Tracker Green DND-26 decreased in cells treated with aPDL1-LAI for 6 h, indicating the disruption of lysosomes by aPDL1-LAI.

It was reported that AuNRs with NIR light could generate heat, which led to cell death. Therefore, the PTT effect of aPDL1-LA was studied in LLC cells using MTT assay. When cells were irradiated with NIR light (2.0 W/cm^2, 5 min), no apparent cell death was observed (Supporting Information Fig. S10). It was proved that the laser we chose was safe. After NIR irradiation, AuNRs, LA, and aPDL1-LA exhibited obvious dose-dependent cytotoxicities, confirming the potential of AuNRs to be used for PTT (Fig. 4G, Supporting Information Fig. S11 and Table S3). The cell viability of aPDL1-LA+NIR was decreased comparing with no NIR irradiation, indicating the antitumor effect of PTT. When cells were treated with LA + NIR and aPDL1-LA+NIR at a concentration equivalent to 20 μg/mL of AuNRs, the cell viabilities were 45.7% and 12.3%, respectively. The aPDL1-LA+NIR exhibited remarkable therapeutic effects due to the targeting ability and PTT effect.

3.4. *In vivo inhibitory effects of aPDL1-LA on lung metastasis*

The combination of PTT with immune-agents will induce potent immune responses[48,49]. According to previous works, PD1 is expressed on immune cells, which can combine with PDL1 (highly expressed on tumor cells). The combination could thus reduce the activity of immune cells, thereby blocking the attack on tumor cells. Tumor cells could hide in this way and survive. Therefore, to study the therapeutic effects of aPDL1-LA to lung metastasis, LLC Lung metastasis models were established by the administration of LLC cells through the tail vein. And then, the tumor nodules and the compact tumor cells in lung tissue (Supporting Information Fig. S12) verified the successful establishment of the lung metastasis model. The animal treatment schedule was shown in Fig. 5A. The inapparent body weight changes demonstrated the safety of the therapeutic agents (Supporting Information Fig. S13). After 2 h intravenous injection of PBS and aPDL1-LA, the lung tissues of mice were exposed to NIR light (2.0 W/cm^2, 5 min), and mice were imaged by the Ti400 thermal imager (Fluke, USA). As shown in Fig. 5B and Supporting Information Fig. S14, the temperature of the lung tissue in mice treated with aPDL1-LA+NIR increased from 34.4 to 43.1 °C, while no noticeable temperature change was observed with PBS. These results suggest the good *in vivo* photothermal effect of aPDL1-LA. To detect the lung metastasis occurrence after the operation, aPDL1-LA was replaced by aPDL1-LAI. With the proliferation of tumor cells, more aPDL1-LAI would combine with PDL1 on tumor cells, causing the increase of fluorescence intensity in lung tissue. As shown in Fig. 5C, with the prolongation of treatment time, the fluorescence intensity decreased gradually, demonstrating the excellent therapeutic effects of aPDL1-LA+NIR. After 16-days' treatment, all tumor-bearing mice were sacrificed, and the appearance of tumor nodules in the lungs was observed after fixation with Bouin's solution (Fig. 5D). The tumor nodules in the lungs of all groups could be clearly seen. The tumor nodules in lungs of mice treated with LA and aPDL1-LA with NIR irradiation were decreased in comparison with no NIR irradiation group, illustrating the therapeutic effect of PTT. What's more, the tumor nodules of the lungs in aPDL1-LA+NIR group were the least due to the synergistic effect of aPDL1 mediated immunotherapy and AuNRs mediated PTT. To further assess the therapeutic effect on lung metastasis, the lungs of five groups were observed through H&E staining (Fig. 5D).

In the process of immunotherapy, cytotoxic T lymphocytes (CTL) play important roles[50]. $CD8^+$ cytotoxic T lymphocytes ($CD3^+CD4^-CD8^+$) can instantly kill tumor cells[51]. And $CD3^+$/$CD4^+$ T-lymphocytes ($CD3^+CD4^+CD8^-$) can not only directly kill tumor cells, but also show the necessity to assist $CD3^+$/$CD8^+$ T-lymphocytes during the process of mediating tumor regression[52]. Simultaneous activation of $CD3^+$/$CD4^+$ T-lymphocytes and $CD3^+$/$CD8^+$ T-lymphocytes is an ideal strategy for immunotherapy. As shown in Fig. 5E, no treatment and LA treated group showed no apparent difference in the ratio of $CD3^+$/$CD4^+$ T-lymphocytes (the rates in Control and LA group were 30.1% and 31.7%, respectively). aPDL1-LA+NIR and LA + NIR showed 45.9% and 36.5% of $CD3^+$/$CD4^+$ T-lymphocytes, which were higher than no NIR irradiation group (the ratios in aPDL1-LA and LA group were 37.8% and 31.7%, respectively). Additionally, the proportion of $CD3^+$/$CD8^+$ T-lymphocytes in aPDL1-LA+NIR group (42.6%)

Table 1 Properties of different nanoparticles.

Sample	DLS diameter (nm)	Polydispersity index (PDI)	Zeta potential (mV)
Hydrogel+IFN-γ+QA	–	–	–31.2 ± 0.5
LA	89.1 ± 7.9	0.33 ± 0.05	–38.9 ± 0.1
aPDL1-LA	92.8 ± 5.7	0.29 ± 0.08	–38.1 ± 0.8

Hydrogel+IFN-γ+QA, thermal responsive hydrogels co-loaded with AP1-QDs, AP2-AuNRs, and interferon-γ (IFN-γ); LA, liposomes-encapsulated AuNRs; aPDL1-LA, anti-PDL1-modified liposomes-encapsulated AuNRs; –, not applicable. Data are presented as mean ± SD (n = 3).

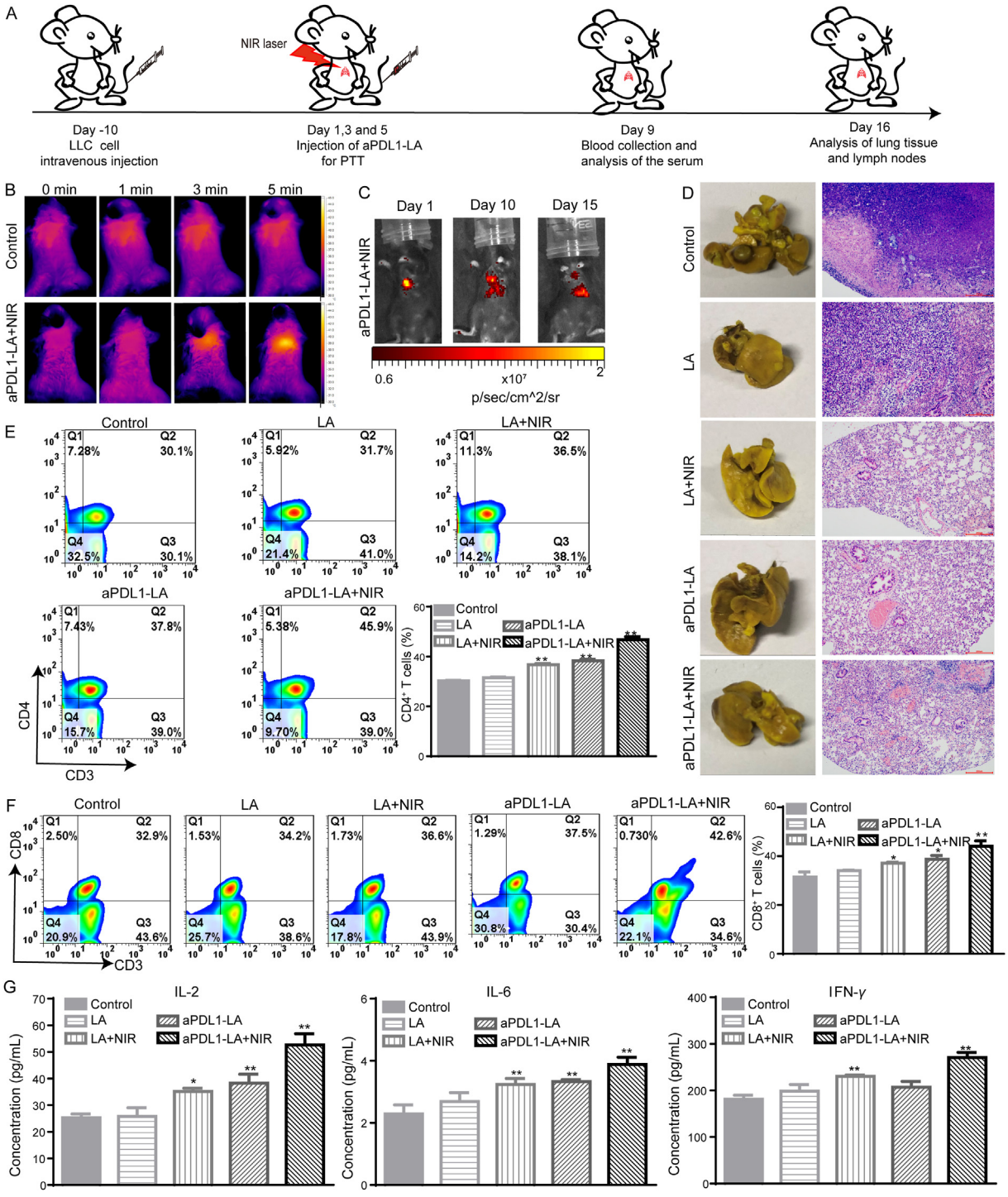

Figure 5 *In vivo* detection and inhibition of lung metastasis after the operation. (A) Schematic diagram of animal experiments; (B) IR thermal images of LLC Lung metastases-bearing mice injected with PBS and aPDL1-LA and then lung tissues were irradiated with 808 nm laser (2.0 W/cm^2 for 5 min); (C) Fluorescence imaging of LLC Lung metastases-bearing mice on Days 1, 10 and 15 post-injection of aPDL1-LA+NIR; (D) Images and H&E staining slices of lung tissues in LLC Lung metastases-bearing mice with different treatments (scale bar = 200 μm); (E) Analysis of CD3$^+$/CD4$^+$ T-lymphocytes in lymph nodes after different treatments by flow cytometry (n = 3, 1 × 10^4 cells measured); Lymph nodes were collected after the treatment, disrupted, stained with anti-CD4-FITC and anti-CD3-PE. (F) Flow cytometry of CD3$^+$/CD8$^+$ T-lymphocytes in lymph nodes after different treatments (n = 3, 1 × 10^4 cells measured) Lymph nodes were collected after the treatment, disrupted, stained with anti-CD8-Percp and anti-CD3-PE; (G) Immune cytokine levels in sera isolated from mice on Day 9 (n = 3). Data are presented as mean ± SD; *P < 0.05, **P < 0.01 compared with control group by ANOVA analysis.

was higher than that in other groups. Furthermore, NIR exposure could also increase the level of $CD3^+/CD8^+$ T-lymphocytes (Fig. 5F). The results indicate that the combination of PTT and immunotherapy can enhance the percentage of cytotoxic T lymphocytes, thus improving therapeutic effects.

Cytokines play an irreplaceable role in tumor immunotherapy. Sera were collected from LLC Lung metastases-bearing mice after 9 days of different treatments to analyze the content of IL-2, IL-6 and IFN-γ. The amounts of IL-2, IL-6 and IFN-γ produced by LA + NIR and aPDL1-LA+NIR were significantly higher than LA and aPDL1-LA (Fig. 5G). The results indicate that aPDL1-LA+NIR can produce more cytokines secretion and thus enhance antitumor effects.

3.5. *In vivo synergistic antitumor effects*

To evaluate the synergistic effect of monitoring and inhibiting postoperative recurrence by combing PTT with immunotherapy, subcutaneous LLC and LLC Lung metastasis model was established at the same time. Hydrogel+IFN-γ+QA was locally

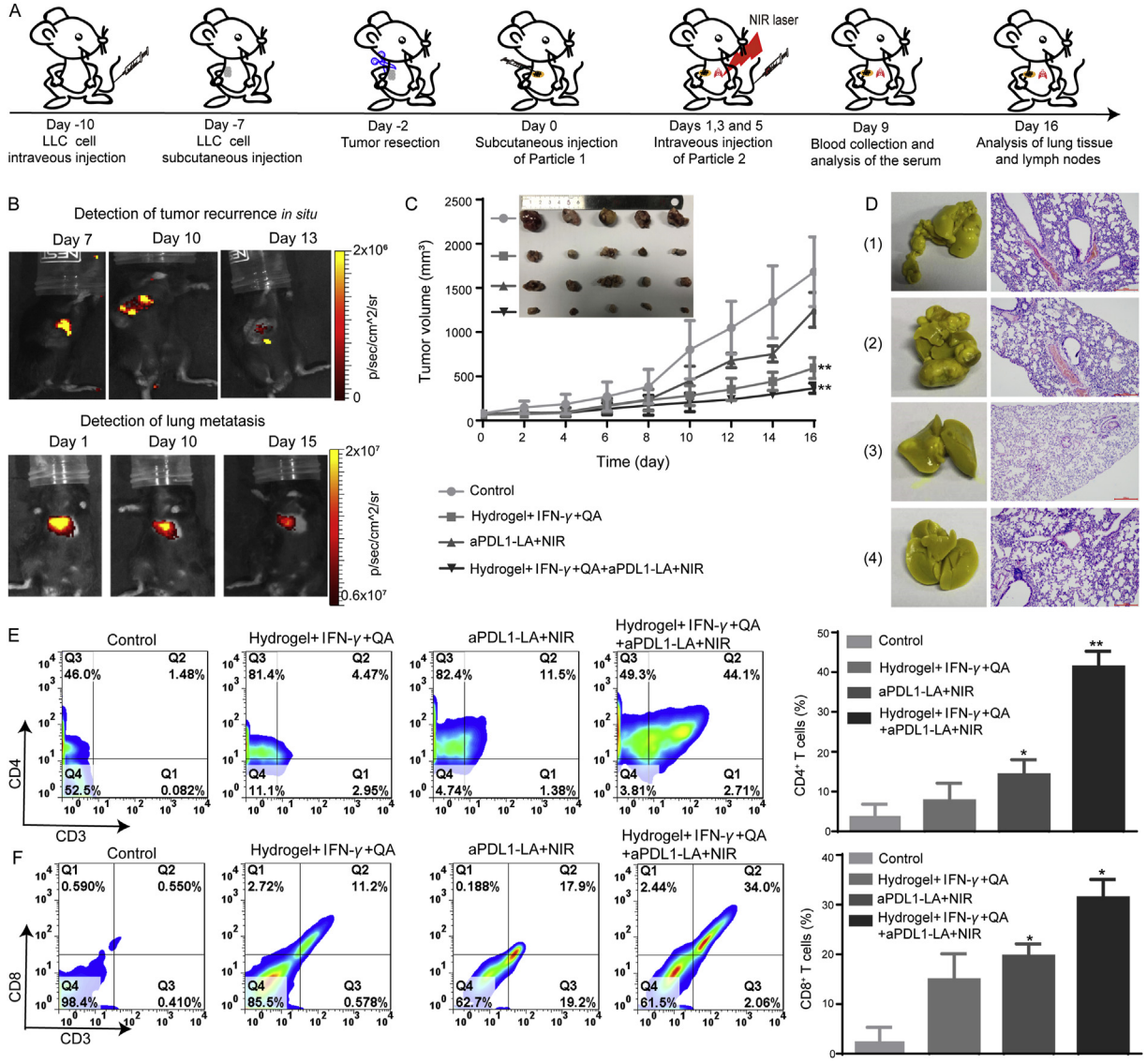

Figure 6 *In vivo* synergistic detection and inhibition of postoperative tumor recurrence. (A) Schematic diagram of animal experiments; Control group: no treatment group; Hydrogel+IFN-γ+QA group: local injection of Hydrogel+IFN-γ+QA; aPDL1-LA+NIR group: intravenous injection of aPDL1-LA with 808 nm laser irradiation; Hydrogel+IFN-γ+QA+aPDL1-LA+NIR group: local injection of Hydrogel+IFN-γ+QA at Day 0 and intravenous injection of aPDL1-LA on Days 1, 3, and 5 with 808 nm laser irradiation; (B) Fluorescence imaging of subcutaneous LLC and LLC Lung metastases-bearing mice, which was subcutaneously injected with Hydrogel+IFN-γ+QA and injected with aPDL1-LAI through tail vein at the same time; (C) Subcutaneous tumor growth curves of mice with different treatments. Inset: photographs of excised subcutaneous tumors ($n = 5$); (D) Images and H&E staining slices of lung tissues (scale bar = 200 μm); (1): Control group; (2): Hydrogel+IFN-γ+QA group; (3): aPDL1-LA+NIR group; (4): Hydrogel+IFN-γ+QA+aPDL1-LA+NIR group. E) Analysis of $CD3^+/CD4^+$ T-lymphocytes in lymph nodes after different treatments by flow cytometry ($n = 3$, 1×10^4 cells measured); (F) Flow cytometry of $CD3^+/CD8^+$ T-lymphocytes in lymph nodes after different treatments ($n = 3$, 1×10^4 cells measured). Data are presented as mean ± SD; $^*P < 0.05$, $^{**}P < 0.01$ compared with untreated group by ANOVA analysis.

injected to detect and inhibit the postoperative occurrence *in situ*. Then aPDL1-LA was injected through the tail vein and exposed to NIR laser to detect and inhibit the growth of lung metastasis. The animal treatment schedule was shown in Fig. 6A. With the increase of tumor volume *in situ*, the fluorescence intensity of tumors in Hydrogel+IFN-γ+QA + aPDL1-LA+NIR group was decreased (Fig. 6B). And then, the fluorescence intensity of lung tissue decreased with the prolongation of treatment time, demonstrating lung cancer metastasis was alleviated. Furthermore, the changes of body weight (Supporting Information Fig. S15A) and H&E staining of main organs (Supporting Information Fig. S17) were insignificant, indicating the safety of therapeutic agents. As demonstrated in Fig. 6C and Supporting Information Fig. S15B, the *in situ* tumor volume of Hydrogel+IFN-γ+QA and Hydrogel+IFN-γ+QA + aPDL1-LA+NIR group reached to 594 and 366.2 mm^3, respectively, obviously smaller than control and aPDL1-LA+NIR group (the tumor volumes were 1683.1 and 1252.2 mm^3, respectively). These results indicated that the combination of Hydrogel+IFN-γ+QA and aPDL1-LA+NIR exhibited evident tumor inhibition *in situ*. The tumor nodules in the lungs of untreated and Hydrogel+IFN-γ+QA groups could be seen, indicating the negative effect on the inhibition of lung cancer metastasis. While the tumor nodules in the lungs of Hydrogel+IFN-γ+QA + aPDL1-LA+NIR group were not appreciable (Fig. 6D). H&E staining showed no difference with this outcome.

According to previous works, activation of DC is essential for cancer immunotherapy[53]. After the treatment, lymph nodes were collected and co-stained with CD11c, CD80 and CD86 antibodies. As illustrated in Supporting Information Fig. S16, Hydrogel+IFN-γ+QA + aPDL1-LA+NIR could induce the highest level of DC maturation than other groups (the percentage was 78.2%). Next, the ratios of $CD3^+/CD4^+$ T-lymphocytes and $CD3^+/CD8^+$ T-lymphocytes were also measured by flow cytometry (FACSCalibur, USA). As shown in Fig. 6E, the rate of $CD3^+/CD4^+$ T-lymphocytes in Hydrogel+IFN-γ+QA + aPDL1-LA+NIR group was as high as 44.1%. However, the proportion in Hydrogel+IFN-γ+QA and aPDL1-LA+NIR group was only 4.47% and 11.5%, respectively. At the same time, Hydrogel+IFN-γ+QA + aPDL1-LA+NIR group showed the highest percentage of $CD3^+/CD8^+$ T-lymphocytes (34.0%) in comparison with other groups (Fig. 6F). These results illustrate the synergistic effect of Hydrogel+IFN-γ+QA + aPDL1-LA+NIR on the activation of DC, generation of $CD3^+/CD4^+$ and $CD3^+/CD8^+$ T-lymphocytes.

In addition, immunohistochemistry (IHC) analysis was conducted to measure the impact on the content of $CD3^+/CD4^+$ T-lymphocytes and $CD3^+/CD8^+$ T-lymphocytes in tumor microenvironment. As shown in Supporting Information Fig. S18, Hydrogel+IFN-γ+QA + aPDL1-LA+NIR group had relatively higher expression of CD4 and CD8 than other groups. Compared with Hydrogel+IFN-γ+QA, Hydrogel+IFN-γ+QA + aPDL1-LA+NIR could induce more activated T cells generation *in vivo*. Immunosuppressive cells (Tregs) are generally recruited into tumor microenvironment[54], thus inhibiting CTLs anti-tumor immunity and DCs activation by secreting numerous cytokines, such as TGF-β or IL-10[55]. In this study, the percentage of Tregs in tumor microenvironment was also measured by IHC analysis to analyze the change of Tregs (Supporting Information Fig. S19).

Sera were collected from subcutaneous LLC and LLC Lung metastasis-bearing mice after 9 days of various treatments to analyze the concentration of IL-2, IL-6 and IFN-γ (Supporting Information Fig. S20). The amount of three immune factors induced by Hydrogel+IFN-γ+QA + aPDL1-LA+NIR was highest, indicating that the synergistic effect of Hydrogel+IFN-γ+QA with aPDL1-LA+NIR could induce more cytokines secretion and thus improve the therapeutic effects on tumor postoperative recurrence, including *in situ* and lung metastasis recurrence.

4. Conclusions

In summary, an efficient synergistic immunotherapy was developed for detection and inhibition of postoperative *in situ* and lung metastasis recurrence. This system could detect and inhibit the postoperative recurrence at the same time. The *in vivo* results showed that this system could exert cooperative antitumor effects on inhibition of postoperative recurrence. All these results indicate that this system can be a promising method for improving therapeutic effects.

Acknowledgments

This work was sponsored by National Key Research and Development Program of China (2017YFA0205104 and 2019YFA0906500), National Natural Science Foundation of China (51873150, 31971300 and 817719709), Tianjin Natural Science Foundation (19JCYBJC28800), Young Elite Scientists Sponsorship Program by Tianjin and the Key project of Tianjin Foundational Research (JingJinJi) Program, China (19JCZDJC64100).

Author contributions

Yingying Zhang and Hanjie Wang designed the research. Yingying Zhang carried out the experiments and performed data analysis. Tiange Wang, Yu Tian and Chaonan Zhang participated part of the experiments. Kun Ge and Jinchao Zhang provided partial animals experiments. Yingying Zhang wrote the manuscript. Hanjie Wang and Jin Chang revised the manuscript. All of the authors have read and approved the final manuscript.

Conflicts of interest

The authors have no conflicts of interest to declare.

Appendix A. Supporting information

Supporting data to this article can be found online at https://doi.org/10.1016/j.apsb.2021.03.035.

References

1. Roayaie S, Jibara G, Tabrizian P, Park JW, Yang JJ, Yan LN, et al. The role of hepatic resection in the treatment of hepatocellular cancer. *Hepatology* 2015;**62**:440–51.
2. Cha CH, Saif MW, Yamane BH, Weber SM. Hepatocellular carcinoma: current management. *Curr Probl Surg* 2010;**47**:10–67.
3. Turajlic S, Swanton C. Metastasis as an evolutionary process. *Science* 2016;**352**:169–75.
4. Krall JA, Reinhardt F, Mercury OA, Pattabiraman DR, Brooks MW, Dougan M, et al. The systemic response to surgery triggers the outgrowth of distant immune-controlled tumors in mouse models of dormancy. *Sci Transl Med* 2018;**10**:eaan3464.
5. Wang C, Sun WJ, Ye YQ, Hu QY, Bomba HN, Gu Z. *In situ* activation of platelets with checkpoint inhibitors for post-surgical cancer immunotherapy. *Nat Biomed Eng* 2017;**1**:0011.

6. Vakkila J, Lotze MT. Opinion—inflammation and necrosis promote tumour growth. *Nat Rev Immunol* 2004;**4**:641−8.
7. Grivennikov SI, Greten FR, Karin M. Immunity, inflammation, and cancer. *Cell* 2010;**140**:883−99.
8. Gao WL, Wang WT, Yao SH, Wu S, Zhang HL, Zhang JS, et al. Highly sensitive detection of multiple tumor markers for lung cancer using gold nanoparticle probes and microarrays. *Anal Chim Acta* 2017;**958**:77−84.
9. Xu YS, Zhang XP, Luan CX, Wang H, Chen BA, Zhao YJ. Hybrid hydrogel photonic barcodes for multiplex detection of tumor markers. *Biosens Bioelectron* 2017;**87**:264−70.
10. Shao K, Wang LF, Wen YT, Wang T, Teng YJ, Shen ZL, et al. Near-infrared carbon dots-based fluorescence turn on aptasensor for determination of carcinoembryonic antigen in pleural effusion. *Anal Chim Acta* 2019;**1068**:52−9.
11. Zhou L, Ji FH, Zhang T, Wang F, Li YC, Yu ZX, et al. An fluorescent aptasensor for sensitive detection of tumor marker based on the FRET of a sandwich structured QDs-AFP-AuNPs. *Talanta* 2019;**197**:444−50.
12. Hamd-Ghadareh S, Salimi A, Fathi F, Bahrami S. An amplified comparative fluorescence resonance energy transfer immunosensing of CA125 tumor marker and ovarian cancer cells using green and economic carbon dots for bio-applications in labeling, imaging and sensing. *Biosens Bioelectron* 2017;**96**:308−16.
13. Saito G, Sadahiro S, Okada K, Tanaka A, Suzuki T, Kamijo A. Relation between carcinoembryonic antigen levels in colon cancer tissue and serum carcinoembryonic antigen levels at initial surgery and recurrence. *Oncology* 2016;**91**:85−9.
14. Wu GS, Feng C, Quan JJ, Wang ZS, Wei W, Zang SQ, et al. *In situ* controlled release of stromal cell-derived factor-1 alpha and antimiR-138 for on-demand cranial bone regeneration. *Carbohydr Polym* 2018;**182**:215−24.
15. Inomata M, Tanaka H, Shimokawa K, Tokui K, Okazawa S, Taka C, et al. A retrospective study analyzing the clinical course of patients with non-small cell lung cancer receiving local or systemic therapy after post-operative recurrence. *Gan To Kagaku Ryoho* 2017;**44**:767−70.
16. Shao JD, Ruan CS, Xie HH, Li ZB, Wang HY, Chu PK, et al. Black-phosphorus-incorporated hydrogel as a sprayable and biodegradable photothermal platform for postsurgical treatment of cancer. *Adv Sci* 2018;**5**:1700848.
17. Kosuge T, Sakamoto Y, Ueno H. Postoperative adjuvant therapy. *J Hepato-Biliary-Pancreatic Sci* 2011;**18**:792−6.
18. Naito M, Tsuboi M. Recent status of postoperative adjuvant chemotherapy after completely resected lung cancer. *Gan To Kagaku Ryoho* 2016;**43**:165−9.
19. Zeng Y, Ruan WL, He JX, Zhang JR, Liang WH, Chen YQ, et al. Adoptive immunotherapy in postoperative non-small-cell lung cancer: a systematic review and meta-analysis. *PLoS One* 2016;**11**:e0162630.
20. Phuengkham H, Song C, Um SH, Lim YT. Implantable synthetic immune niche for spatiotemporal modulation of tumor-derived immunosuppression and systemic antitumor immunity: postoperative immunotherapy. *Adv Mater* 2018;**30**:1706719.
21. Mellman I, Coukos G, Dranoff G. Cancer immunotherapy comes of age. *Nature* 2011;**480**:480−9.
22. Saeed M, Gao J, Shi Y, Lammers T, Yu HJ. Engineering nanoparticles to reprogram the tumor immune microenvironment for improved cancer immunotherapy. *Theranostics* 2019;**9**:7981−8000.
23. Shen J, Xiao ZG, Zhao QJ, Li MX, Wu X, Zhang L, et al. Anti-cancer therapy with TNF alpha and IFN gamma: a comprehensive review. *Cell Prolif* 2018;**51**:e12441.
24. Lv Q, He CL, Quan FL, Yu SJ, Chen XS. DOX/IL-2/IFN-gamma co-loaded thermo-sensitive polypeptide hydrogel for efficient melanoma treatment. *Bioact Mater* 2018;**3**:118−28.
25. Melero I, Berman DM, Aznar MA, Korman AJ, Gracia JLP, Haanen J. Evolving synergistic combinations of targeted immunotherapies to combat cancer. *Nat Rev Cancer* 2015;**15**:457−72.
26. Chen WF, Qin M, Chen XY, Wang Q, Zhang ZR, Sun X. Combining photothermal therapy and immunotherapy against melanoma by polydopamine-coated Al_2O_3 nanoparticles. *Theranostics* 2018;**8**:2229−41.
27. Wang M, Song J, Zhou FF, Hoover AR, Murray C, Zhou BQ, et al. NIR-triggered phototherapy and immunotherapy *via* an antigen-capturing nanoplatform for metastatic cancer treatment. *Adv Sci* 2019;**6**:1802157.
28. Chen Q, Xu LG, Liang C, Wang C, Peng R, Liu Z. Photothermal therapy with immune-adjuvant nanoparticles together with checkpoint blockade for effective cancer immunotherapy. *Nat Commun* 2016;**7**:13193.
29. Zhang D, Wu Tt, Qin XY, Qiao Q, Shang LH, Song QL, et al. Intracellularly generated immunological gold nanoparticles for combinatorial photothermal therapy and immunotherapy against tumor. *Nano Lett* 2019;**19**:6635−46.
30. Tang XC, Tan LW, Shi K, Peng JR, Xiao Y, Li WT, et al. Gold nanorods together with HSP inhibitor-VER-155008 micelles for colon cancer mild-temperature photothermal therapy. *Acta Pharm Sin B* 2018;**8**:587−601.
31. Li DD, Zhang M, Xu F, Chen YZ, Chen BF, Chang Y, et al. Biomimetic albumin-modified gold nanorods for photothermo-chemotherapy and macrophage polarization modulation. *Acta Pharm Sin B* 2018;**8**:74−84.
32. Zhao YT, Tong LP, Li Y, Pan HB, Zhang W, Guan M, et al. Lactose-functionalized gold nanorods for sensitive and rapid serological diagnosis of cancer. *ACS Appl Mater Interfaces* 2016;**8**:5813−20.
33. Chen YS, Zhao Y, Yoon SJ, Gambhir SS, Emelianov S. Miniature gold nanorods for photoacoustic molecular imaging in the second near-infrared optical window. *Nat Nanotechnol* 2019;**14**:465−72.
34. Powles T, Eder JP, Fine GD, Braiteh FS, Loriot Y, Cruz C, et al. MPDL3280A (anti-PD-L1) treatment leads to clinical activity in metastatic bladder cancer. *Nature* 2014;**515**:558−62.
35. Qian HF, Dong CQ, Weng JF, Ren JC. Facile one-pot synthesis of luminescent, water-soluble, and biocompatible glutathione-coated CdTe nanocrystals. *Small* 2006;**2**:747−51.
36. Zhang LM, Xia K, Lu ZX, Li GP, Chen J, Deng Y, et al. Efficient and facile synthesis of gold nanorods with finely tunable plasmonic peaks from visible to near-IR range. *Chem Mater* 2014;**26**:1794−8.
37. Nikoobakht B, El-Sayed MA. Preparation and growth mechanism of gold nanorods (NRs) using seed-mediated growth method. *Chem Mater* 2003;**15**:1957−62.
38. Li FQ, Mei H, Gao Y, Xie XD, Nie HF, Li T, et al. Co-delivery of oxygen and erlotinib by aptamer-modified liposomal complexes to reverse hypoxia-induced drug resistance in lung cancer. *Biomaterials* 2017;**145**:56−71.
39. Gao Y, Gu SE, Zhang YY, Xie XD, Yu T, Lu YS, et al. The architecture and function of monoclonal antibody-functionalized mesoporous silica nanoparticles loaded with mifepristone: repurposing abortifacient for cancer metastatic chemoprevention. *Small* 2016;**12**:2595−608.
40. Gu CC. Quantum dots-based fluorescence resonance energy transfer biosensor for monitoring cell apoptosis. *Luminescence* 2017;**32**:1186−91.
41. Xia YS, Song L, Zhu CQ. Turn-on and near-infrared fluorescent sensing for 2,4,6-trinitrotoluene based on hybrid (gold nanorod)-(quantum dots) assembly. *Anal Chem* 2011;**83**:1401−7.
42. Liang GX, Pan HC, Li Y, Jiang LP, Zhang JR, Zhu JJ. Near infrared sensing based on fluorescence resonance energy transfer between Mn:CdTe quantum dots and Au nanorods. *Biosens Bioelectron* 2009;**24**:3693−7.
43. Showalter A, Limaye A, Oyer JL, Igarashi R, Kittipatarin C, Copik AJ, et al. Cytokines in immunogenic cell death: applications for cancer immunotherapy. *Cytokine* 2017;**97**:123−32.
44. Sim GC, Radvanyi L. The IL-2 cytokine family in cancer immunotherapy. *Cytokine Growth Factor Rev* 2014;**25**:377−90.

45. Morgan DA, Ruscetti FW, Gallo R. Selective *in vitro* growth of T lymphocytes from normal human bone marrows. *Science* 1976;**193**:1007−8.
46. Guo YQ, Xu F, Lu TJ, Duan ZF, Zhang Z. Interleukin-6 signaling pathway in targeted therapy for cancer. *Cancer Treat Rev* 2012;**38**:904−10.
47. Yuba E, Kanda Y, Yoshizaki Y, Teranishi R, Harada A, Sugiura K, et al. pH-sensitive polymer-liposome-based antigen delivery systems potentiated with interferon-gamma gene lipoplex for efficient cancer immunotherapy. *Biomaterials* 2015;**67**:214−24.
48. Li L, Yang SX, Song LJ, Zeng Y, He T, Wang N, et al. An endogenous vaccine based on fluorophores and multivalent immunoadjuvants regulates tumor micro-environment for synergistic photothermal and immunotherapy. *Theranostics* 2018;**8**:860−73.
49. Zhang YY, Chen HB, Wang HJ, Wang TG, Pan HZ, Ji WY, et al. A synergistic cancer immunotherapy nano-system for preventing tumor growth. *Chem Eng J* 2020;**380**:122472.
50. Barry M, Bleackley RC. Cytotoxic T lymphocytes: all roads lead to death. *Nat Rev Immunol* 2002;**2**:401−9.
51. Durgeau A, Virk Y, Corgnac S, Mami-Chouaib F. Recent advances in targeting CD8 T-cell immunity for more effective cancer immunotherapy. *Front Immunol* 2018;**9**:14.
52. Gliwinski M, Piotrowska M, Iwaszkiewicz-Grzes D, Urban-Wojciuk Z, Trzonkowski P. Therapy with $CD4^{+}CD25^{+}$ T regulatory cells—should we be afraid of cancer?. *Współczesna Onkol* 2019;**23**:1−6.
53. Liu X, Feng ZJ, Wang CR, Su Q, Song HJ, Zhang CN, et al. Co-localized delivery of nanomedicine and nanovaccine augments the postoperative cancer immunotherapy by amplifying T-cell responses. *Biomaterials* 2020;**230**:119649.
54. Curiel TJ, Coukos G, Zou LH, Alvarez X, Cheng P, Mottram P, et al. Specific recruitment of regulatory T cells in ovarian carcinoma fosters immune privilege and predicts reduced survival. *Nat Med* 2004;**10**:942−9.
55. Dong X, Yang A, Bai Y, Kong DL, Lv F. Dual fluorescence imaging-guided programmed delivery of doxorubicin and CpG nanoparticles to modulate tumor microenvironment for effective chemo-immunotherapy. *Biomaterials* 2020;**230**:119659.